NASA/TM-20220008028

Impact of Future Low-Emissions Combustor Technology on Acoustic Scaling Laws

Duane McCormick
Raytheon Technologies Research Center, East Hartford, Connecticut

Lennart S. Hultgren
Glenn Research Center, Cleveland, Ohio

Jeffrey M. Mendoza
Raytheon Technologies Research Center, East Hartford, Connecticut

June 2022

NASA STI Program . . . in Profile

Since its founding, NASA has been dedicated to the advancement of aeronautics and space science. The NASA Scientific and Technical Information (STI) Program plays a key part in helping NASA maintain this important role.

The NASA STI Program operates under the auspices of the Agency Chief Information Officer. It collects, organizes, provides for archiving, and disseminates NASA's STI. The NASA STI Program provides access to the NASA Technical Report Server—Registered (NTRS Reg) and NASA Technical Report Server—Public (NTRS) thus providing one of the largest collections of aeronautical and space science STI in the world. Results are published in both non-NASA channels and by NASA in the NASA STI Report Series, which includes the following report types:

- TECHNICAL PUBLICATION. Reports of completed research or a major significant phase of research that present the results of NASA programs and include extensive data or theoretical analysis. Includes compilations of significant scientific and technical data and information deemed to be of continuing reference value. NASA counter-part of peer-reviewed formal professional papers, but has less stringent limitations on manuscript length and extent of graphic presentations.

- TECHNICAL MEMORANDUM. Scientific and technical findings that are preliminary or of specialized interest, e.g., "quick-release" reports, working papers, and bibliographies that contain minimal annotation. Does not contain extensive analysis.

- CONTRACTOR REPORT. Scientific and technical findings by NASA-sponsored contractors and grantees.

- CONFERENCE PUBLICATION. Collected papers from scientific and technical conferences, symposia, seminars, or other meetings sponsored or co-sponsored by NASA.

- SPECIAL PUBLICATION. Scientific, technical, or historical information from NASA programs, projects, and missions, often concerned with subjects having substantial public interest.

- TECHNICAL TRANSLATION. English-language translations of foreign scientific and technical material pertinent to NASA's mission.

For more information about the NASA STI program, see the following:

- Access the NASA STI program home page at http://www.sti.nasa.gov

- E-mail your question to help@sti.nasa.gov

- Fax your question to the NASA STI Information Desk at 757-864-6500

- Telephone the NASA STI Information Desk at 757-864-9658

- Write to:
  NASA STI Program
  Mail Stop 148
  NASA Langley Research Center
  Hampton, VA 23681-2199

NASA/TM-20220008028

Impact of Future Low-Emissions Combustor Technology on Acoustic Scaling Laws

Duane McCormick
Raytheon Technologies Research Center, East Hartford, Connecticut

Lennart S. Hultgren
Glenn Research Center, Cleveland, Ohio

Jeffrey M. Mendoza
Raytheon Technologies Research Center, East Hartford, Connecticut

National Aeronautics and
Space Administration

Glenn Research Center
Cleveland, Ohio 44135

June 2022

Acknowledgments

The material presented here is based upon work supported by the National Aeronautics and Space Administration Advanced Air Transport Technology Project, under NRA Contract NNC16CA39C. The authors thank Walter Borst, John Costello, Wookyung Kim, Justin Locke, Lance Smith, and Jordan Snyder of Raytheon Technologies Research Center and Scott Liljenberg and Ramons Reba of Pratt & Whitney for discussions and contributions to the research effort.

This work was sponsored by the Advanced Air Vehicle Program
at the NASA Glenn Research Center

Level of Review: This material has been technically reviewed by technical management.

This report is available in electronic form at http://www.sti.nasa.gov/ and http://ntrs.nasa.gov/

Impact of Future Low-Emissions Combustor Technology on Acoustic Scaling Laws

Duane McCormick
Raytheon Technologies Research Center
East Hartford, Connecticut 06108

Lennart S. Hultgren
National Aeronautics and Space Administration
Glenn Research Center
Cleveland, Ohio 44135

Jeffrey M. Mendoza
Raytheon Technologies Research Center
East Hartford, Connecticut 06108

Abstract

The overall goal of a recent research project at the Raytheon Technologies Research Center, under National Aeronautics and Space Administration sponsorship, was to develop a first-of-its-kind database of detailed unsteady measurements characterizing noise sources of far-term advanced low-emissions aero-combustors. The program addressed the need for fundamental combustion-noise experiments which, in the near term, enable improvements to reduced-order models for use in system level noise assessments at the preliminary design stage for advanced air transport vehicles. In addition, optical measurement techniques were refined and validated for usage at the higher pressures and temperatures relevant to future combustor designs. In the long term, results from this program can be utilized to validate high-fidelity prediction methods suited for detailed multi-disciplinary acoustics/emissions combustor design. This paper concentrates on one aspect of the overall project, namely an examination of the legacy scaling laws for broadband combustor noise.

I. Introduction

The development of future subsonic-transport-aircraft configurations and propulsion systems targeting dramatic reductions in noise and emissions will require consideration of currently subdominant noise sources. Future propulsion systems are envisioned to have an increasingly higher bypass ratio from larger fans combined with much smaller cores, with high-efficiency, ultra-clean burning, fuel-flexible combustors [1]. The continuing trend toward higher bypass ratios and sustained investments in noise-mitigation technologies have significantly reduced jet and fan noise, respectively, for modern turbofans as well as elevating the (future) importance of core noise [2]. Of the core-noise sources (compressor, combustor, and turbine), combustor noise is the one potentially most negatively affected, i.e., increased in strength, by the expected turbofan-design changes and, consequently, is generally recognized as a key technical challenge in meeting future noise targets. Combustor, or combustion, noise is a low-frequency broadband component and already can make a significant contribution to the aft-quadrant overall noise signature at approach conditions for current-generation high-bypass-ratio turbofan engines. The situation is further aggravated by the low-frequency character of combustion noise which makes it less amenable to shielding by the airframe.

Because of the historical ranking of noise sources by importance, the jet-exhaust- and fan-noise areas have benefited from decades of sustained research investments in acoustic modeling, simulation, experimental diagnostics, and noise control technologies, while aeroengine-combustor acoustics has received comparatively little attention. As a result, acoustic assessments of future low-emissions combustor technology currently rely on semi-empirical OEM-developed tools rooted in 1970s-era combustor designs, and little, or no, capability exists today to reliably assess the acoustic impact of emerging combustor technologies. Meanwhile, low-emissions combustor technology has been rapidly advancing through joint NASA-Industry efforts over the past 5 years [3, 4]. Fundamental combustion noise experiments therefore are needed, in the near term, to enable improved reduced-order models for use in system-level noise assessments at the preliminary design stage and, in the long term, to address validation needs of high-fidelity prediction methods suited for detailed multi-disciplinary acoustics/emissions combustor design. Without complementary combustor/combustion-noise research, there is a significant risk of setting far-term combustor-technology directions that unnecessarily compromise community-noise impact and thereby jeopardize overall environmental goals.

In response to this need for fundamental experiments, a research project was carried out at the Raytheon Technologies Research Center (RTRC)[a] [5] in partnership with NASA (NRA Contract NNC16CA39C). The aim of the work was threefold, namely: (i) to develop a first-of- its-kind database of detailed unsteady measurements characterizing noise sources of far-term advanced low-emissions aero-combustors under realistic operating conditions; (ii) to advance/validate optical measurement techniques—such as chemiluminescence for unsteady heat release and tunable diode laser absorption spectroscopy (TDLAS) for unsteady temperature—for usage at the higher pressures and temperatures relevant to future combustor environments; and (iii) to examine how well existing acoustic-power scaling laws—used for farfield semi-empirical noise predictions—capture the combustor broadband-noise characteristics under far-term operating conditions, as well as identify improvements needed for the legacy models. Detailed multi-point unsteady heat-release measurements, in combination with unsteady pressure measurements, were obtained providing noise-source data and statistical characterization of the direct-noise field for a representative N+3 combustor design, as well as for a reference N design. The N+3 notation indicates three future generations beyond the current state-of-the-art design, N. This characterization [5] provides critical understanding of how the dominant source locations, length scales and convective features differ in current and future advanced, low-emissions combustors. Limited TDLAS measurements at the combustor-rig exit were also obtained in order to provide input to future indirect-noise modeling activities.

This paper reports on the third objective above, namely the assessment of the impact of the N+3 radical departure from N combustor designs, operating conditions, fuel-air distribution, and flame anchoring techniques, on legacy semi-empirical noise prediction methods [6]. An analysis of measured power spectra, verifying the scaling principles underpinning current reduced-order models, is presented. Modifications to extend and generalize such principles to future advanced combustors is proposed. The reader is referred to Ref. 5 for details about other aspects of the testing.

II. Background

A. Low-Emission Combustor Technologies

Legacy combustor designs all have generic features that create a rich front-end to provide robust flame stabilization and a variety of secondary/dilution air holes along the length of the combustor to provide high-combustion efficiency (i.e. complete CO burnout) as well as tailoring of the temperature profile entering the turbine. Throughout the years this combustor design was refined and became known as a rich-quench-lean (RQL) combustor. Some manufacturers have started to move away from this design given challenges with minimizing emissions, primarily nitrogen oxide (NO_x), but this basic combustor design still maintains a strong presence in legacy products and in some cases even N+1 combustor designs [7, Fig. 1]. In these RQL combustors, fuel and air are mixed using high shear created by a multi-pass injector at the front of the combustor. The rich flame is stabilized by the recirculation zones created by strong residual swirl from the mixer. Downstream of the stabilization region, the flame is quenched by dilution-air jets to create an overall lean flame for the remainder of the fuel burn.

TECHNOLOGY BENEFITS*	TECHNOLOGY GENERATIONS (Technology Readiness Level = 4-6)		
	N+1 (2015)	N+2 (2020**)	N+3 (2025)
Noise (cum margin rel. to Stage 4)	-32 dB	-42 dB	-71 dB
LTO NOx Emissions (rel. to CAEP 6)	-60%	-75%	-80%
Cruise NOx Emissions (rel. to 2005 best in class)	-55%	-70%	-80%
Aircraft Fuel/Energy Consumption‡ (rel. to 2005 best in class)	-33%	-50%	-60%

* Projected benefits once technologies are matured and implemented by industry. Benefits vary by vehicle size and mission. N+1 and N+3 values are referenced to a 737-800 with CFM56-7B engines, N+2 values are referenced to a 777-200 with GE90 engines

** ERA's time-phased approach includes advancing "long-pole" technologies to TRL 6 by 2015

‡ CO_2 emission benefits dependent on life-cycle CO_{2e} per MJ for fuel and/or energy source used

Fig. 1 NASA 2013 goals for next-generation subsonic-transport aircraft performance, emissions, and noise

NASA, RTRC, and Pratt & Whitney recently have explored combustor designs to meet the challenging N+3 low-emissions and higher-thermal-efficiency requirements (NRA Contract NNC14CA30C) [3]. The N+3 combustor designed under that contract leverages an N+2 combustor architecture developed under earlier joint efforts (NRA

[a]Previously known as United Technologies Research Center (UTRC)

Contracts NNC10CA11C [8] and NNC10BA12B [9], see also Ref. 10), but is a scaled variant to meet the more stringent N+3 requirements, see Fig. 1. The emissions requirement is achieved by lean burning throughout the combustor and the higher thermal efficiency is obtained through a higher overall pressure ratio (OPR). Figure 2 schematically compares the basic features of a generic RQL combustor, Panel (a), to those of the proposed design, a so-called axially controlled stoichiometry (ACS) combustor, Panel (b). The ACS combustor introduces axial staging using separate pilot and main injectors, with distinct functions and designs. The pilot and main injectors both mix fuel and air. The pilot injector provides a stable lean flame for low power conditions and the main injector is fueled at higher power conditions and is stabilized by hot products from the pilot flame. A further discussion of modern low-emissions technologies is provided in the review article by Liu et al. [11].

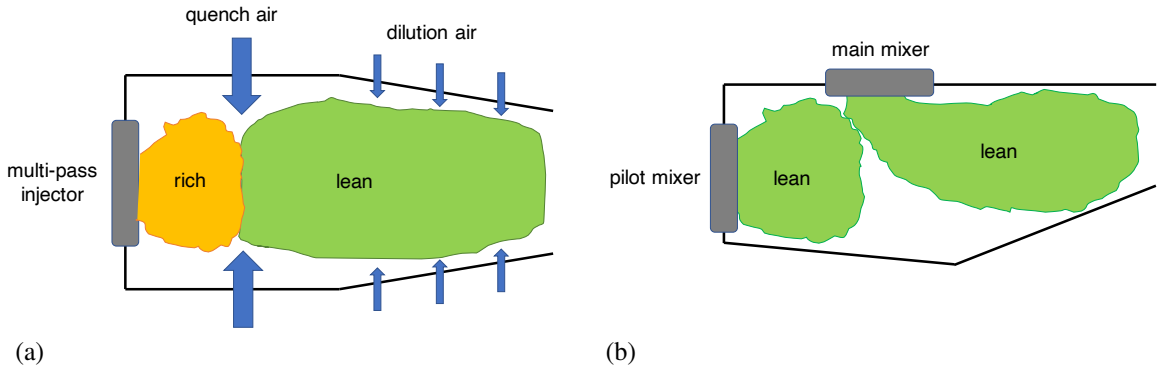

Fig. 2 Schematic illustration of combustor designs: (a) RQL and (b) ACS

Table 1 Relevant characteristics of aerocombustor generations

	Generation			
	Legacy	N and N+1	N+2	N+3
Front-End Equivalence Ratio, ϕ	stoichiometric	rich	lean	lean
Fuel Injection	non-PM*	non-PM	non-PM / PM	non-PM / PM
Flame Anchoring	RZSF**	RZSF	RZSF / RJIC***	RZSF / RJIC

* PM: premixed ** RZSF: recirculating-zone stabilized flame *** RJIC: reacting jet in crossflow

Table 1 summarizes some of the key differences between legacy, current-generation, and future-generation aerocombustors. These changes in key characteristics are expected to influence the nature of the combustion noise sources and thus impact the ability of legacy modeling tools to accurately predict the generation of combustor/combustion noise. Of these characteristics, as will be seen later in this paper, the flame anchoring difference has the largest effect.

B. Combustor/Combustion Noise Physics and Prediction

In the context of aeroengine applications, the unsteady combustion process generates both so-called 'direct' and 'indirect' combustor noise. The former is acoustic pressure fluctuations resulting directly from the unsteady heat release in the combustion region(s). In contrast, the latter is acoustic pressure fluctuations that are produced in the downstream engine-internal flow path due to the effect of rapid meanflow variation on convected entropy, vorticity, and compositional disturbances that also are created by the unsteady combustion process. Recent reviews of the area and further references can be found in Refs. 12–15. The relative importance of these two components is still uncertain. However, up to this point, it has generally been assumed by industry practitioners that the direct noise is dominant in real-life applications, but this situation is not certain to remain so in the future due to the trend towards lean-lean combustion technologies. However, the current experimental setup [5] is geared towards investigating the direct-noise source mechanism (and so is the analysis presented herein).

Methods for predicting direct combustor/combustion noise can be broadly categorized in a hierarchy of approaches, similar in principle to those used in the more mature jet- and fan-noise areas. At the highest level of fidelity are approaches which aim to solve the fully-compressible, reactive Navier-Stokes equations via large-eddy simulation (LES). This approach directly captures the acoustic field while also resolving the unsteady reactive flow [16–18]. With

these most advanced computational tools, detailed flame/turbulence interactions can be captured, but the quality of the results are still limited by the caliber of turbulent sub-grid scale models and combustion sub-models. These methods are computationally very expensive and at present have limited utility as original-equipment manufacturer (OEM) design tools. The next lower level of fidelity is offered by hybrid methods, which rely on acoustic analogies in various forms, where equivalent sources describing sound generation are introduced in acoustic propagation models. Here, the space-time characteristic of the acoustic sources are first computed or estimated using a computational-fluid-dynamics (CFD) models ranging from low-Mach-number, reactive LES to unsteady Reynolds-averaged Navier-Stokes (URANS) solvers, neither of which can directly capture the acoustics. Analytical or finite-element (FE) based tools are then used to solve linearized propagation models to determine the acoustic field. Although hybrid methods for combustion noise prediction have made significant strides in recent years, their application has been mainly limited to canonical problems and simplified geometries. Significant further development and validation is needed before such methods can be reliably used for acoustic assessment of advanced combustor technologies, especially with turnaround times suitable for design. Due to the aforementioned challenges, OEM combustor noise assessments have relied heavily on semi-empirical methods. Such methods aim to use physics-based foundations to define scaling laws and rig and engine data to determine model constants, directivity functions, and spectra.

Semi-empirical predictions have proven valuable for many OEM applications and commonly include methods that can be traced back to models developed in the 1970s by Mathews and Rekos [19] and Ho and Doyle [20] based on OEM-proprietary engine and rig data. In 1980, the latter method was adopted by the Society of Automotive Engineers International (SAE) as the SAE ARP876 [21] technical standard for the prediction of noise from conventional combustors installed in gas-turbine engines. This standard also forms the kernel of the GECOR core-noise module in the NASA Aircraft Noise Prediction Program (ANOPP) [22, 23]. However, the databases underpinning these methods are relatively narrow in scope with limited geometric variations. Thus, their applicability to revolutionary new combustor architectures, as outlined above, is questionable at best without significant model enhancements to address emerging technologies.

C. ANOPP/SAE and Mathews-Rekos Scaling Laws

In the present work, measured dynamic pressure data for the N and N+3 configurations are compared to results from two legacy combustor/combustion-noise prediction techniques, namely the semi-empirical ANOPP/SAE [20–23] and Mathews-Rekos[19] methods. In particular, the comparisons center on the scaling laws for the total radiated acoustic power in these methods. A recent general discussion of semi-empirical prediction of direct combustor noise can be found in Refs. 6 and 15.

The acoustic overall power level in the ANOPP/SAE-model is given by

$$OAPWL = 10\log_{10}\left[\dot{m}_b c_o^2 \left(\frac{T_4 - T_3}{T_3}\right)^2 \left(\frac{P_3}{P_o}\right)^2\right] + K_{\mathrm{SAE}} - 10\log_{10}(\Pi_{ref})\,, \tag{1}$$

where $P_o = 101.325\,\mathrm{kPa}$ (14.6959 psi) and $c_o = 340.294\,\mathrm{m/s}$ (1116.45 ft/s) are the ambient static pressure and speed of sound—here given by the corresponding international sea-level static (SLS) values since actual ambient conditions are not relevant for a test rig; $\dot{m}_b$ is the burner massflow rate; T_3 and T_4 are the total temperatures at the combustor inlet and exit; P_3 is the total pressure at the combustor inlet; $K_{\mathrm{SAE}} = -60.53\ldots$ is a data-fitted constant; and $\Pi_{ref} = 1 \times 10^{-12}\,\mathrm{W}$ is a reference power.

The acoustic overall power level in the Mathews-Rekos model, which will be referred to as the P&W model in what follows, is given by

$$OAPWL = 10\log_{10}\left[\frac{(P_3 A_b)^2}{N_f}\left(\frac{FP_b}{A_b}\right)^4\left(\frac{T_{st}}{T_3}\right)^2 F_b^2\right] + K_{\mathrm{P\&W}}\,, \tag{2a}$$

where A_b is the burner cross-sectional area, N_f is the number of injectors (or burner cans in a cannular combustor), $FP_b = \dot{m}_b\sqrt{T_3}/P_3$ is a burner flow parameter (related to the corrected massflow rate), F_b is the fuel-to-air ratio, and

$$T_{st} = T_3\left(1 + \frac{H_f F_{st}}{c_p T_3}\right) \tag{2b}$$

is the stochiometric flame temperature, with H_f, F_{st}, and c_p being the fuel heating value, the stochiometric fuel-to-air-ratio, and specific heat at constant pressure, respectively. Note that, in contrast to Eq. (1), the quantity inside the square bracket in Eq. (2a) does not have the dimension of power. Consequently, the value of the data-fitted constant $K_{\mathrm{P\&W}}$ depends on the unit system used. For the choice of customary U.S. engineering units, $K_{\mathrm{P\&W}} = 132$ [19].

III. Experiment

The objective of the project [5] was, in part, to statistically characterize and compare the internal direct-noise fields for N and N+3 aerocombustors under realistic operating conditions in order to provide crucial understanding of how the source structures, i.e., source strengths, characteristic length scales, convective features, etc., vary between current and future advanced, low-emissions combustors. The campaign was carried out using the RTRC high-pressure, high-temperature Variable Resonance Acoustic Screening Capability (VRASC) test rig.

The project benefited significantly from a partial overlap with an earlier-started NASA-UTRC/RTRC N+3-combustor development effort [3], in that their test-section geometry, as well as their combustor-dynamics mapping, could be leveraged for this test campaign. The additional instrumentation ports (optical and other) needed by this project was then also available for usage in the later phases of their testing. This exemplifies the potential synergies achievable by select linking of government-industry research projects.

A. Test Sections

In broad strokes, the N+3-combustor project [3] used a multistep process to design the rig test section. First, an engine cycle and a core size must be selected. A turbofan cycle defines, among other things, the fan pressure ratio (FPR), overall pressure ratio (OPR), the bypass ratio (BPR), and the total temperature at the turbine inlet guide vanes (IGV) at the aerodynamical design point (ADP) for a target engine. The ADP is normally the top-of-climb (TOC) condition. The core size is generally expressed in terms of the ADP corrected massflow rate at the compressor exit and, in combination with the cycle, determines the ADP engine thrust, as well as the effective IGV flow area. The Pratt & Whitney (P&W) SGTF2065 engine cycle for the Massachusetts Institute of Technology (MIT) D8.6 concept aircraft (see [24] for a brief description of both) was selected, but now with a core size of 2 lbm/s (0.907 kg/s). Second, Pratt & Whitney subsequently performed a mean-line turbomachinery analysis, using proprietary component models, that provided an accurate and complete set of off-design operating conditions as well as geometric constraints for the N+3 combustor. Pratt & Whitney next determined approximate combustor dimensions, commensurate with compressor-exit and turbine-inlet geometries, determined by the mean-line analysis, and with adequate combustor-section length and volume for its aerodynamic and aerothermal functions, based on company design rules and experience. Third, these Pratt & Whitney results were then used as inputs for detailed CFD analysis of an ACS N+3 combustor at RTRC/UTRC. Finally, a rig test-section could be developed [3]. Its design represents a single combustor sector of a 14-sector annular combustor consistent with the P&W-SGTF2065 engine cycle with a core size of 2 lbm/s (0.907 kg/s). The side-wall inserts provide an approximate annular segment (a true annular segment would have circular-arced outer-diameter and inner-diameter walls rather than the flat walls used here).

For the current project [5], the N+3 combustor test-section design was modified with a relatively large chemiluminescence imaging window. For the reference N configuration, the top and bottom walls of the N+3 combustor sector were replaced with dilution jet inserts designed to approximate a typical RQL configuration while maintaining the combustor flow splits of the N+3 configuration, see Fig. 3. Either combustor configuration was installed in the VRASC

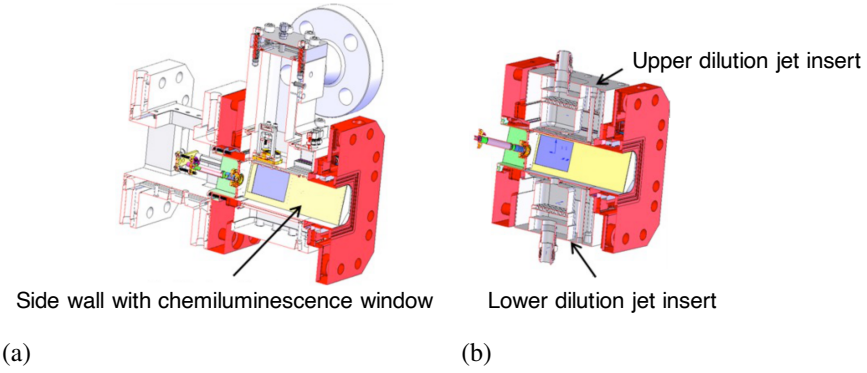

Fig. 3 VRASC combustor sectors: (a) N+3-generation ACS configuration; (b) N-generation RQL configuration

test rig, which is shown in Fig. 4, during different phases of the campaign. There are separate heated air streams that feed the centerline (the pilot mixer for the N+3 configuration and the sole injector for the N configuration) and the side branches (the main mixer for the N+3 configuration and the dilution jets for the N configuration). Downstream of

the combustor section is a side branch pipe (labeled 'VRASC tube' in the figure) of variable length that is controlled by a movable plunger. The maximum length of the plunger stroke is about 54 inches (1.37 m). The variable tube length enables evaluation of the sensitivity, at different frequencies, to thermo-acoustic instability of a fuel/air mixer by changing the longitudinal acoustic modes in the combustion section. For the current investigation, the VRASC plunger was fixed at a location that minimizes in-band acoustic modes so that the broadband, direct noise field can be studied. Downstream of the VRASC tube is a variable-area choke providing a realistic downstream boundary condition, typical of an aerocombustor.

The N+3 combustor development project [3] screened four different pilot fuel atomizers for their dynamic response under cruise and approach operating conditions. Of these four atomizers, the so-called 'air-blast' pilot fuel atomizer was selected for use with the current project [5] due to its apparent reduced propensity to thermo-acoustic instability.

B. Instrumentation

Figure 5 shows the locations and numbering of the dynamic pressure instrumentation. The dynamic pressure measurements are all made with infinite-tube probe (ITP) sensors that are calibrated at atmospheric conditions and data-matched to a frequency-based acoustic model for post-test corrections. The ITP measuring locations include the pilot and main plenums (P5 and P6, respectively), pilot bulkhead (P7), aft-test section (P8), and VRASC flange (P9). Other locations, not shown in the figure, include the end of the VRASC tube and its plunger face (P10).

The project [5] also performed unsteady heat release (UHR) imaging using chemiluminescence techniques. These measurements were used to determine dominant source locations and integral length scales, convective speeds and propagation directions of UHR structures, as well as to compute an associated direct-noise field. In addition, during part of the investigation, an instrumentation flange allowing for Tunable Diode Laser Absorption Spectroscopy (TDLAS) and dual-thermocouple probe measurements was inserted between combustor and aft test sections (replacing the light grey section between the red and mid-grey sections in Fig. 5). However, since those aspects of the investigation [5] are not the focus of the present paper, the techniques and instrumentation involved are not discussed here.

C. Test Matrix

The relevant operating points for the N+3 and N combustors from an airport-community noise perspective, namely takeoff, climb and approach for each, are illustrated qualitatively in Fig. 6 in terms of the total temperature, T_3, and total pressure, P_3, at the compressor exit. The red symbols are conditions defined by the N+3 combustor-development project [3] and the blue symbols correspond to a P&W PW6000 engine cycle, which was selected as representative for N-generation combustors. The Pratt & Whitney PW6000 is a modern high-bypass-ratio turbofan engine developed for 100-passenger-class single-aisle aircraft (such as the Airbus A318).

In general, the desired absolute temperatures and pressures could be dialed in with errors less than one percent and seven percent, respectively, in the rig, which is a quite acceptable result. The exception was the N+3 approach condition, where a lower pressure was needed to achieve stable operation. This 'modified' N+3 approach condition (black symbol in Fig. 6) has a total pressure that is about 30 percent lower than desired, but the total temperature is within 1.3 percent of the cycle value. This particular N+3 condition will be referred to without its qualifier from here on, except when needed for clarity.

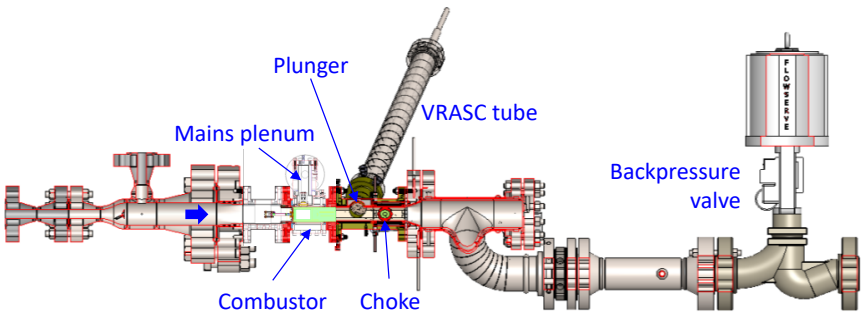

Fig. 4 RTRC VRASC test rig

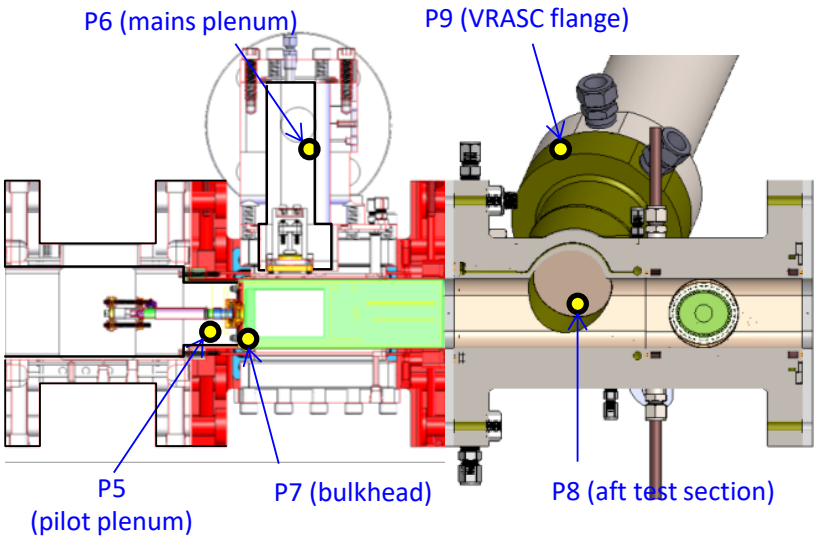

Fig. 5 Dynamic pressure instrumentation

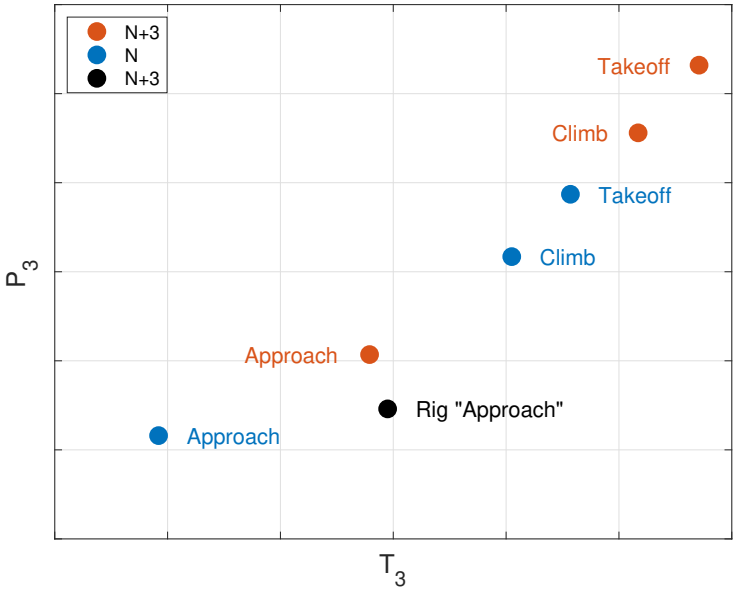

Fig. 6 N and N+3 operating conditions

In addition, at each nominal operating point, sweeps of the fuel-to-air-ratio (FAR) parameter F_b, the flow parameter FP_b (related to the corrected massflow rate at the burner inlet), P_3, and T_3 were performed independently while holding all other combustor conditions approximately constant. This range of operating points and associated parameter variations allowed an assessment of legacy combustor-noise scaling laws for the acoustic power, see Section II.C.

IV. Results

The presentation in this paper only covers a subset of the overall-project [5] results, namely the examination of the legacy semi-empirical scaling laws described above in Section II.C. The reader is referred to the project report [5] for details of other aspects of the investigation.

For each rig set point, digital time histories of the ITP pressure signals were acquired using a sampling rate of 16,384 Hz for a duration of 30 s. Thus, each sequence contains just under half-a-million data points. Auto-spectra were then obtained by applying the MATLAB function `pwelch` to the time histories, using Hann windowing and a segment length of 16,384, with no overlap. Consequently, the spectra have a frequency resolution (or binwidth) of 1 Hz and each is the result of 30 averages. The ITP transfer-function corrections were then applied to the spectra. The ITP transfer function was only determined up to 5,000 Hz and, hence, the corrected spectra are only available in the frequency range of 1–5,000 Hz. Even though this upper limit is less than the 8,192 Hz range of the raw ITP spectra, it is sufficiently higher than the frequency range of interest for broadband combustor noise, say $\lesssim$ 1,600 Hz. For simplicity, the qualifier 'corrected' will be dropped hereafter when discussing dynamic pressure spectra—unless the qualifier 'raw' is used all spectra are ITP-transfer-function corrected.

A. Narrowband Amplitude and Sound-Power-Level Spectra

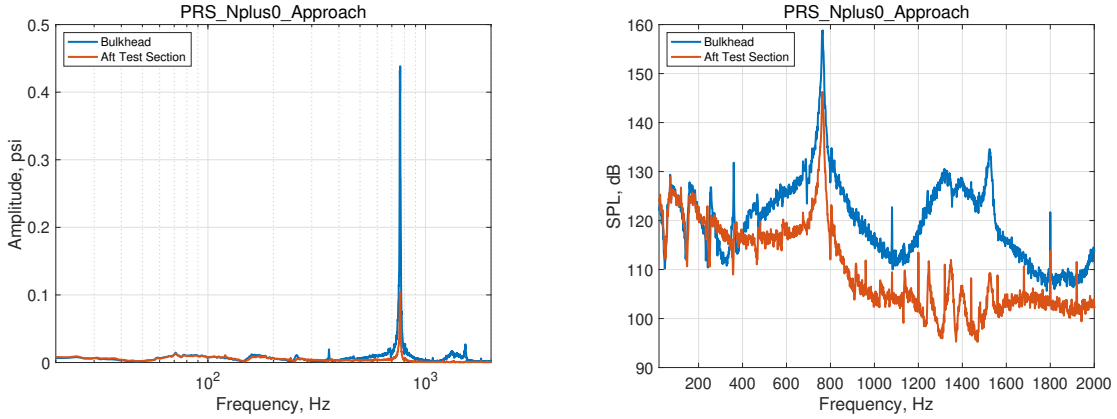

(a) (b)

Fig. 7 Dynamic pressure spectra for the N approach condition: (a) linear amplitude and (b) SPL

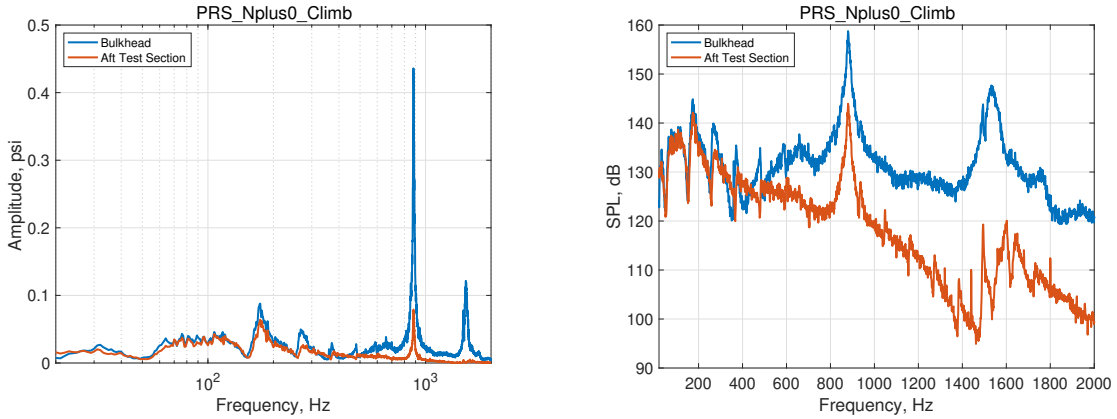

(a) (b)

Fig. 8 Dynamic pressure spectra for the N climb condition: (a) linear amplitude and (b) SPL

Figures 7–9 and 10–12 show dynamic-pressure spectra for the N and N+3 configurations, respectively, corresponding to the approach, climb, and takeoff cycle points for the frequency range of 20–2,000 Hz. The blue and red curves represent the bulkhead and aft-test-section locations, respectively. The (a) Panels in these figures show the 'traditional' linear pressure amplitude spectra, whereas the (b) Panels show the corresponding sound-pressure-level (SPL) spectra. Note that the effective tone-binwidth adjustment has been removed in the SPL spectra since the broadband noise is of primary interest in that case.

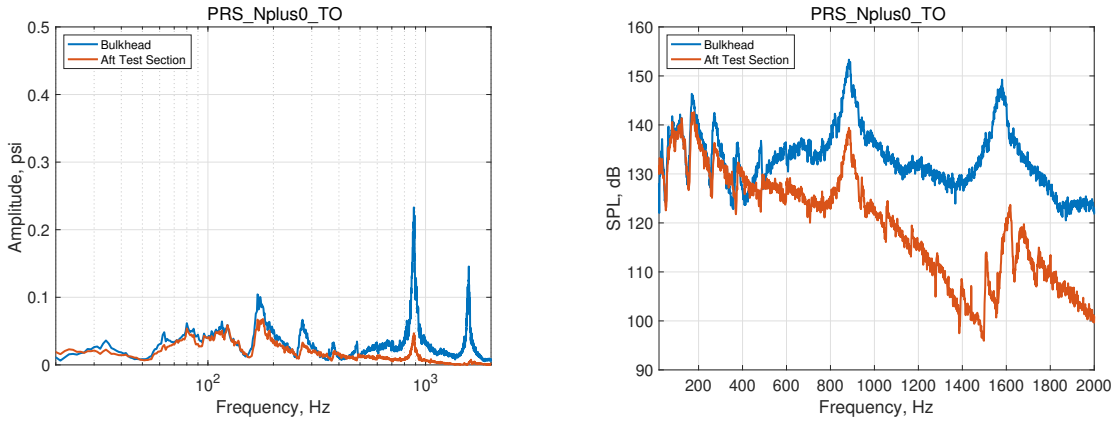

(a) (b)

Fig. 9 Dynamic pressure spectra for the N takeoff condition: (a) linear amplitude and (b) SPL

An accurate finite-element acoustic (FEA) model of the combustor section and test-rig piping was developed using COMSOL. In particular, the acoustic impedance (resistance and reactance) of the fuel-atomizer sub-model was validated using a flowing impedance tube test. Further details about the development and validation of the FEA model can be

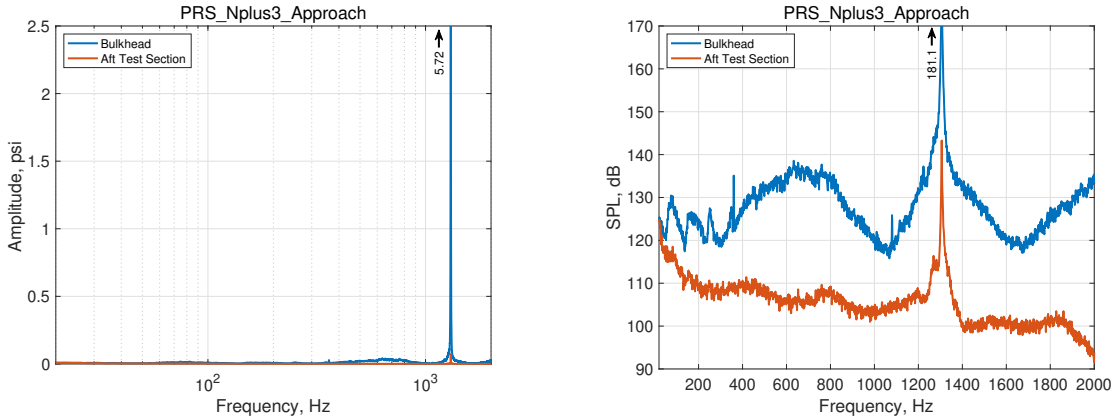

(a) (b)

Fig. 10 Dynamic pressure spectra for the N+3 approach condition: (a) linear amplitude and (b) SPL

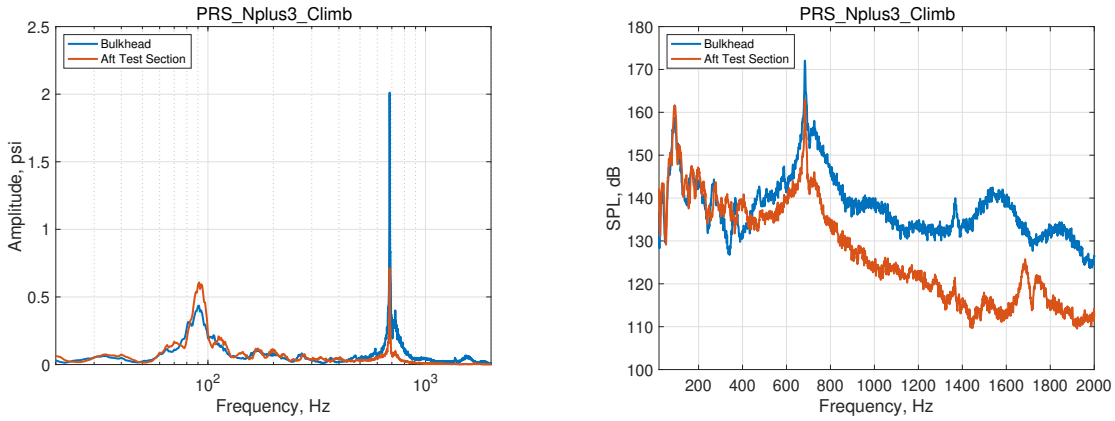

(a) (b)

Fig. 11 Dynamic pressure spectra for the N+3 climb condition: (a) linear amplitude and (b) SPL

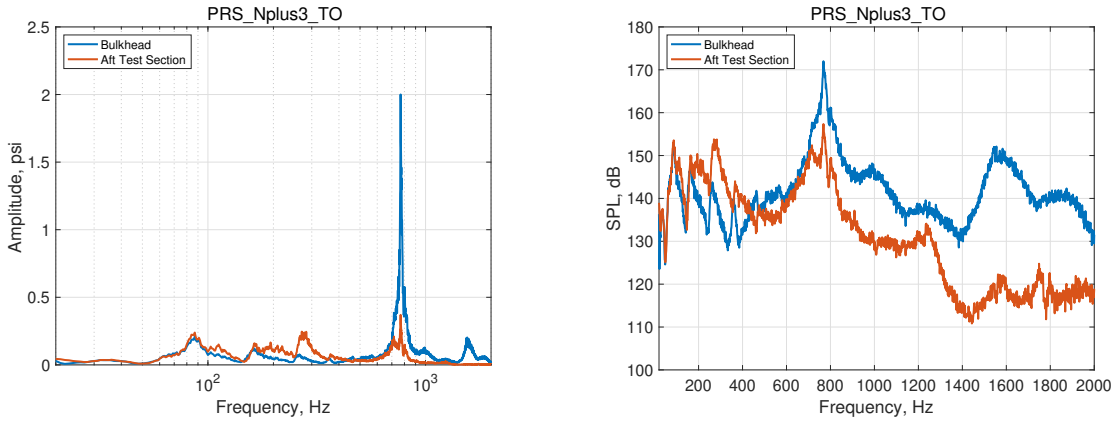

(a) (b)

Fig. 12 Dynamic pressure spectra for the N+3 takeoff condition: (a) linear amplitude and (b) SPL

found in the project report [5]. The main purpose of the FEA model was to provide numerical basis functions for an acoustic direct-noise computation based on the measured unsteady heat release (this aspect is not reported on in the present paper, however), but the FEA model additionally provides a better understanding of the measured dynamic pressures.

The FEA model showed a particular strong resonant response to the applied forcing (mimicking the unsteady heat release) when the test-section (bulkhead-to-choke) half-wavelength longitudinal mode and the VRASC (bulkhead-to-piston) full-wavelength mode frequencies coincide. Depending on the operating conditions, this resonance frequency roughly falls between 700–900 Hz. Thus, the strong (or strongest) discrete tone observable in Figs. 7–9, 11, and 12 are manifestations of this resonance. The very strong tone in Fig. 10 is an outlier in this respect, but is most likely associated with a confluence of higher-harmonic longitudinal test-section and VRASC bulk modes.

Since the plunger is not perfectly sealed inside the VRASC tube, the small leakage allows for an acoustic coupling with the volume behind the plunger. As a result, a full-wavelength mode from the bulkhead to the end of the VRASC tube occurs at around 90–100 Hz, nearly independent of the plunger stroke position. The spectral hump, roughly centered about 90 Hz, seen in Fig. 11(a) is clearly an effect of this bulk mode. Also, the 'N-shaped' modulations, below about 400 Hz, visible in some of the SPL spectra in Figs. 7–12 are likely caused by this particular bulk mode and its harmonics.

Furthermore, by comparing the rig results shown in these figures, it is clear that both the discrete tone and broadband levels are higher in the N+3 configuration compared to the N one. This observation is in line with the commonly held belief that the higher unsteadiness expected in lean-lean combustor designs will lead to higher acoustic levels. However, it is important to note that neither of these two test-section configurations directly corresponds to any existing Pratt & Whitney aeroengine combustor. This is particularly so for the N+3 configuration, which is purely an early fundamental research concept to explore the challenges and potential benefits of future advanced combustor concepts.

B. One-Third-Octave Sound-Power-Level Spectra

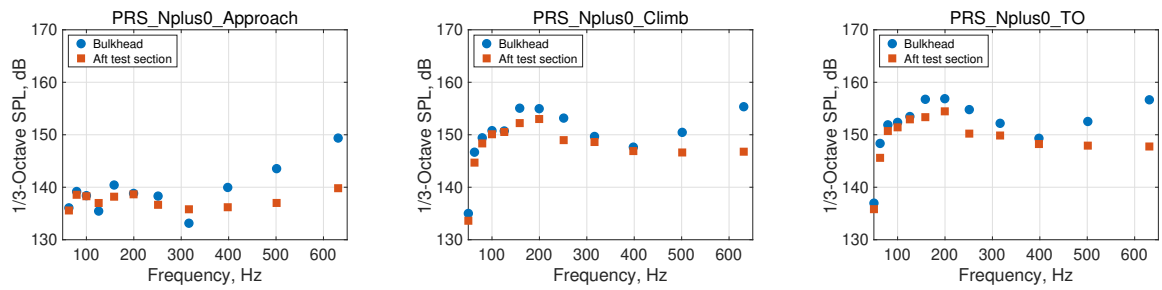

(a) (b) (c)

Fig. 13 1/3-octave SPL spectra for the N configuration: (a) approach, (b) climb and (c) takeoff

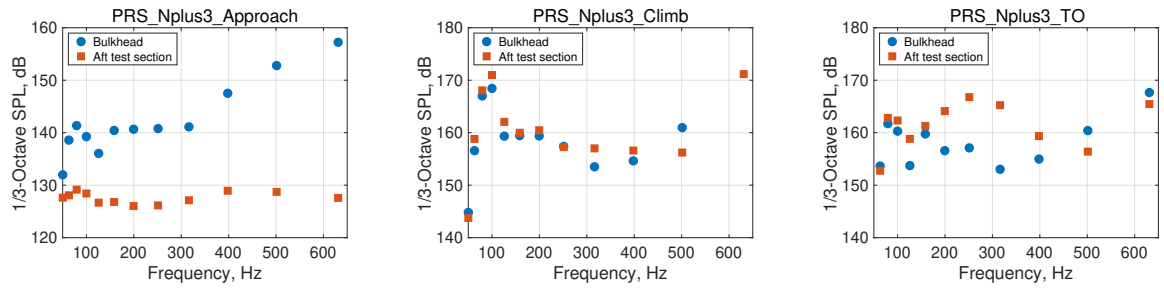

Fig. 14 1/3-octave SPL spectra for the N+3 configuration: (a) approach, (b) climb and (c) takeoff

The narrowband SPL spectra shown in Panel (b) of Figs. 7–12 can be summed up, or reapportioned, to yield 1/3-octave SPL spectra traditionally used in legacy prediction methods for broadband combustor noise. Of course, the resulting spectra are here heavily influenced by the presence of the discrete tones for bands with center frequencies larger than about 650 Hz. Consequently, only bands for a with center-frequencies lower than this value are considered here.

Figure 13 shows the 1/3-octave SPL spectra for the N configuration. As before, the blue and red colors (solid circles and squares, respectively) represent the bulkhead and aft-test-section locations. Panels (a), (b), and (c) are for the approach, climb, and takeoff cycle conditions, respectively. It appears that the discrete tone has a much stronger influence on adjacent frequencies at the bulkhead location. This is also apparent in the narrowband plots in Section IV.A through the larger 'haystacks' around the tone for the bulkhead measurements. The conclusion is that here the 500 Hz and 630 Hz bands are 'contaminated' and should be excluded when calculating an overall sound-power level associated with broadband noise. The contamination is less for the aft-test-section measurements, but it is still present and the same conclusion is valid for these measurements too. By visual inspection of Fig. 13, it follows that the broadband noise, on an 1/3-octave basis, peaks at about 200 Hz for all three cycle points.

Figure 14 shows the corresponding 1/3-octave SPL spectra for the N+3 configuration, with the color/symbol key being the same as in the previous figure. Generally, because of the higher unsteadiness the situation is here much less clear cut. However, it is clear that the 500 Hz and 630 Hz bands are also here contaminated by secondary effects due to the presence of the strong discrete tones. It is also clear that, at least for the climb and takeoff conditions, the 80 Hz and 100 Hz bands are here contaminated, by the plunger-leakage bulk mode.

C. Overall Broadband Sound Pressure Level

For this paper, it was decided to only use contributions from 1/3-octave bands spanning from 50 Hz to 400 Hz, inclusive, when estimating the overall sound pressure level (OASPL) associated with the broadband noise. The contamination due to the plunge-leakage mode was removed from the results by replacing the contributions from the 80 Hz and 100 Hz bands with linearly interpolated 1/3-octave SPL values. This weighted arithmetic-averaging technique in the SPL space is equivalent to using a weighted geometric-averaging method for the corresponding physical mean-pressure-square quantities. Table 2 shows the result of this adjustment procedure for the estimated broadband

Table 2 Aft-Test-Section Broadband OASPL Estimates

Generation	N			N+3		
Cycle Condition	Approach	Climb	Takeoff	Approach	Climb	Takeoff
OASPL (original), dB	146.9	159.5	161.0	137.6	174.0	172.4
OASPL (adjusted), dB	146.4	159.1	160.6	137.3	169.1	171.6

combustor-noise contributions to the OASPL in the aft test section. In four of the six cases shown, the adjustment is less than -0.5 dB, which can be considered as insignificant and is consistent with the results shown in Figs. 13 and 14. The adjustment is significant (about -5 dB) for the N+3 climb condition. For the N+3 takeoff condition the modification is moderate (about -1 dB).

The estimation procedure for the OASPL associated with broadband noise in Ref. 5 was somewhat different. In that report, a frequency response curve obtained by the FEA model was applied in order to remove, or minimize, the influence of the longitudinal duct modes. Their approach certainly made the spectra appear more regular in the

frequency range of interest, but may not have adjusted the 'power' level to reflect only the broadband component. In addition, they also included the 500 Hz band in the OASPL estimates.

D. Net Radiated Acoustic Power

The net downstream radiated power by plane waves in a uniform duct is given by

$$\Pi =< pu > A_b = \frac{A_b}{\rho_m c_m} < \left[p_+^2(\xi_+) - p_-^2(\xi_-)\right] >= \frac{A_b}{\rho_m c_m}\left[< p_+^2(\xi_+) > - < p_-^2(\xi_-) >\right], \tag{3}$$

where $p_\pm(\xi_\pm)$, with $\xi_\pm = x_m - (U \pm c_m)t$, represent downstream and upstream traveling plane waves, x and t are the streamwise coordinate and time, the subscript 'm' denotes the measurement location, A_b is the duct cross-sectional area, and the brackets (<...>) denote the ensemble average of the enclosed quantity.

For situations where the upstream propagating wave can be neglected as being of small amplitude compared to the downstream propagating wave, the downstream radiated acoustic power can be approximated by

$$\Pi \approx \frac{< p^2 > A_b}{\rho_m c_m}. \tag{4}$$

Equation (4) applies to the situation considered here, except close to the resonance conditions described in Section IV.A.

Hence, the overall power level is given by

$$OAPWL \equiv 10\log_{10}(\Pi/\Pi_{ref}) \approx 10\log_{10}\left(\frac{< p^2 > A_b}{\rho_m c_m \Pi_{ref}}\right) = OASPL - 10\log_{10}\left(\frac{\rho_m c_m}{\rho_o c_o}\right) + 10\log_{10}\left(\frac{P_{ref}^2 A_b}{\rho_o c_o \Pi_{ref}}\right). \tag{5}$$

Equation (5) forms the basis for the evaluation of the legacy semi-empirical scaling laws using the broadband OASPL estimated from the experimental measurements. The nondimensional third term of the last member of this equation is a constant for a given burner. Note that in the current rig setup, the N and N+3 configurations have identical cross-sectional areas, so this constant has the same value for all cases considered herein. The second term of the last member of this equation varies with test-point conditions and simply reflects the acoustic impedance difference between the test-section and reference conditions; ρ_m and c_m are the static mean density and adiabatic speed of sound at the measuring location and ρ_o and c_o are the corresponding quantities for the SLS condition (cf. Section II.C). The impedance ratio, ζ, can be approximated as follows

$$\zeta \equiv \frac{\rho_{sm} c_m}{\rho_o c_o} = \frac{P_{sm}}{P_o}\sqrt{\frac{\gamma_m T_o}{\gamma T_{sm}}} \approx \frac{P_{tm}}{P_o}\sqrt{\frac{\gamma_m T_o}{\gamma T_{tm}}} \approx \frac{P_{tm}}{P_o}\sqrt{\frac{T_o}{T_{tm}}}, \tag{6}$$

where 's' and 't' have been added to some of the subscripts to indicate static and total quantities, respectively when needed for clarity; $\gamma = 1.4$ is the ratio of the specific specific heats at constant pressure and volume at SLS; γ_m ($\leq \gamma$) is the corresponding ratio at the measuring location. Due to the low Mach number of the mean flow in a combustor, the static pressure and temperature can then be approximated by their corresponding total values. In practice, the difference between γ_m and γ can also safely be ignored. At the aft-test-section location, $P_{tm} = P_4$ and $T_{tm} = T_4$, where P_4 and T_4 are the combustor-exit total pressure and temperature. Due to the (small) mean pressure drop across the combustor, $P_4 \lesssim P_3$. At the bulkhead location, $T_{tm} = T_{4F}$, where T_{4F} is the combustor front-end total temperature, which can be estimated based on the pilot fuel-to-air ratio and the assumptions of complete combustion and adiabatic wall conditions.

Consequently, when plotting the sum of the two first terms of the last member of Eq. (5), using Eq. (6), as a function of either the first term of Eqs. (1) or (2a), the data points should cluster along a straight line of unity slope if the scaling laws are valid. In contrast to Ref. 5, the evaluation here is carried out using the aft-test-section measurements rather than the bulkhead measurements. The rationale for this is simply that it is quite possible that the bulkhead measurements are more affected by pseudo sound than the aft-test-section ones. That is, because of the higher unsteadiness expected in the former location, a portion of the measured signals could there be hydrodynamical pressure fluctuations rather than acoustic ones. It can also be argued that the aft-test-section measurements are more relevant when the main interest are acoustic disturbances that ultimately would emanate from an aeroengine and then propagate to the farfield.

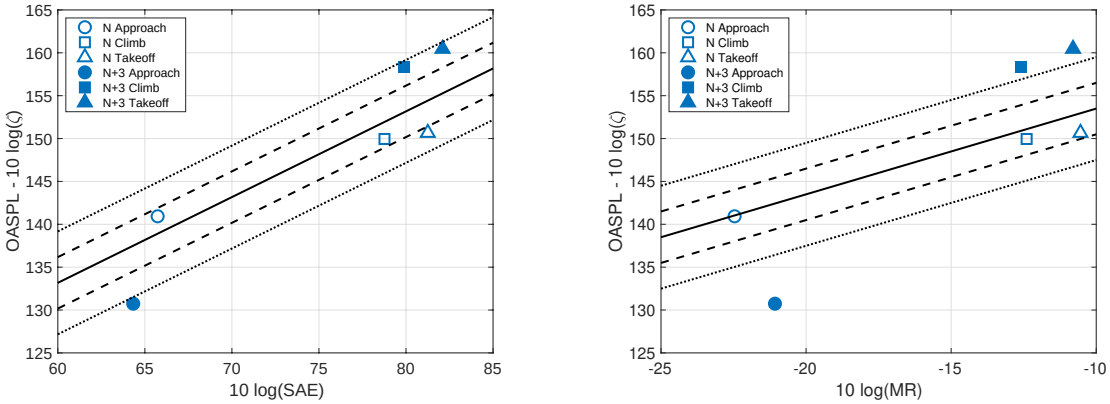

Fig. 15 Comparison of measurements with legacy scaling laws for both N and N+3 cycle points: (a) ANOPP/SAE model and (b) Mathew-Rekos model

E. A First Comparison with Legacy Scaling Laws

Figure 15 shows comparisons based on the estimated downstream-transmitted broadband acoustic power and the two legacy scaling laws based on the N and N+3 cycle points. The ordinate represents the sum of the two first terms (i.e., the non-constant ones) of the last member of Eq. (5). The abscissa represents the first term of Eqs. (1) and (2a) in Panels (a) and (b), respectively. SAE and MR used in the abscissa titles are shorthand notations for the arguments of the base-ten logarithm in the corresponding scaling laws. As already pointed out, for a scaling law to be valid, the data points should scatter around a unity-slope straight line, i.e.,

$$y = x + C\,, \tag{7}$$

when plotted in this manner. Least-square fits, using the data shown in this figure, lead to $C_{SAE} = 73.17$ and $C_{MR} = 163.49$. The solid black lines in Fig. 15 represent the linear fits and the black dashed and dotted lines indicate ± 3 dB and ± 6 dB bands. Both legacy scaling laws, perhaps not surprisingly, appear to work reasonably well for the N configuration. The situation is less clear for the N+3 configuration, however. The N+3 trends are not unreasonable when compared with the ANOPP/SAE scaling law, but of course the data and predictions deviate more than in the N case. Since the N+3 approach conditions is quite an outlier in Fig. 15(b), no clear conclusion can be drawn at this point about the applicability of the Mathews-Rekos model to the N+3 case.

F. The Effect of Parameter Sweeps

The validity of each legacy scaling law was further examined by performing limited parameter sweeps anchored at each nominal operating point. The FAR (F_b), the combustor inlet total temperature (T_3) and pressure (P_3), and the flow parameter (FP_b) were individually varied while keeping the other approximately constant.

Figure 16 shows the results for the FAR sweeps. The blue, red, gold, and purple colors indicate the nominal value at each operating point, a 10 %, a 20 %, and a 30 % increase, respectively. The circles, squares, and triangles denote the approach, climb, and takeoff conditions. The open and closed symbols indicate N and N+3 configurations, respectively. The lines are based on the estimated constants and bands above, Section IV.E. For the N case, the acoustic power increases as expected with increasing FAR value. The accuracy of the fit essentially remains unchanged for both scaling laws in this rig configuration. In contrast to the N case, the FAR increase is accompanied by a decrease in the estimated acoustic power for both the N+3 climb and takeoff conditions, which is opposite of what is expected from the scaling laws. This deviation is hypothesized to be due to the relatively weaker flame anchoring of the main combustion flame in the N+3 case compared to the N case—reacting-jet-in-cross-flow versus recirculating-zone-stabilized-flame anchoring. This weaker anchoring in the N+3 configuration is likely more prone to low-frequency oscillations as well as being more sensitive to the presence of longitudinal bulk modes. As the FAR is increased, the resulting higher combustor temperature (T_4) presumably stabilizes the flame and thereby reduces the noise for these N+3 operating conditions. The N+3 approach condition is clearly an outlier for both comparisons. However, it is possible that the broadband contribution to the acoustic power is underestimated by the current procedure for this particular case and operational

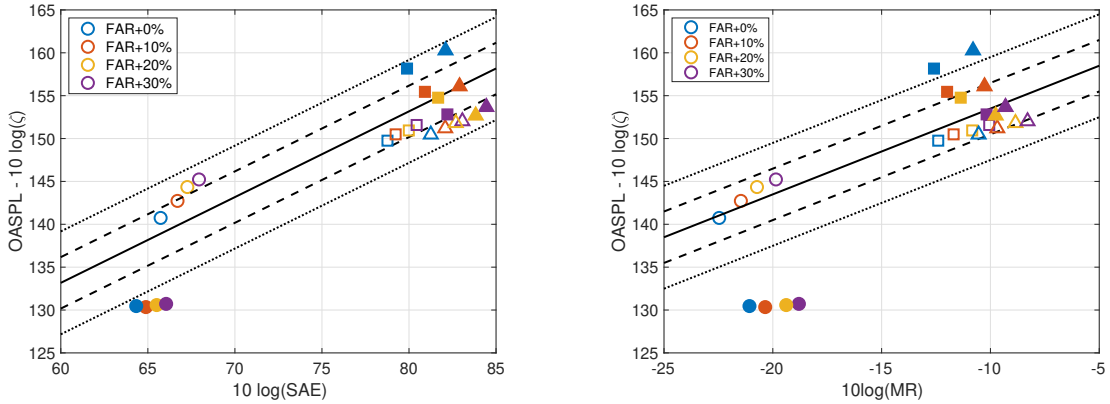

Fig. 16 Comparison of measurements with legacy scaling laws for both N and N+3 cycle points, FAR sweeps: (a) ANOPP/SAE model and (b) Mathew-Rekos model

point because the discrete tone occurs at essentially twice the frequency compared to the other operational points. By including 1/3-octave band contributions up to and including 800 Hz for the N+3 approach condition (only), it is found that the OASPL estimates for that particular condition would be increased by just under 2 dB compared to what is shown in this figure. This certainly would improve the situation somewhat for the ANOPP/SAE comparison, but it is not a sufficient adjustment to substantially better the Mathews-Rekos comparison.

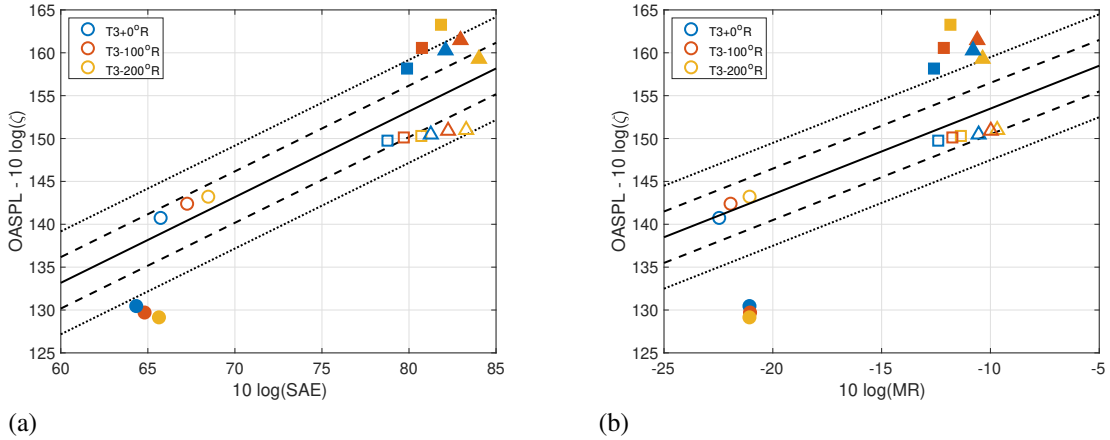

Fig. 17 Comparison of measurements with legacy scaling laws for both N and N+3 cycle points, T_3 sweeps: (a) ANOPP/SAE model and (b) Mathew-Rekos model

Figure 17 shows the results for the combustor inlet total temperature (T_3) sweeps. The blue, red, and gold colors indicate the nominal value at each operating point, a 100 °R and a 200 °R decrease, respectively. The other keys are the same as in Fig. 16. Again, the N-case acoustic-power estimates are reasonably well predicted by both legacy scaling laws—with the Mathews-Rekos scaling being slightly better. Continuing the summation of the contributions up to and including the 800-Hz band for the N+3 approach case, would, as would have been the case in Fig. 16, somewhat improve the comparison with the SAE/ANOPP scaling law. Furthermore, the large increase in the acoustic power indicated by the (N+3 climb) gold square is spurious. It is simply a reflection of the fact that the plunger-leakage mode not only becomes stronger but also moves towards slightly lower frequencies as T_3 is decreased from its cycle value—the fixed-filter procedure used here simply fails to correct for this behavior. An adoptive filtering technique could be employed to remedy this, but it was felt that it was best to not have too many adjustable parameters in this initial analysis of the data. The fixed-filter worked well for the N+3 takeoff condition, however.

Figure 18 shows the results for the combustor inlet total temperature (P_3) sweeps. The blue, red, and gold colors indicate the nominal value at each operating point, a δ increase and decrease, and a 2δ decrease. The other keys are the

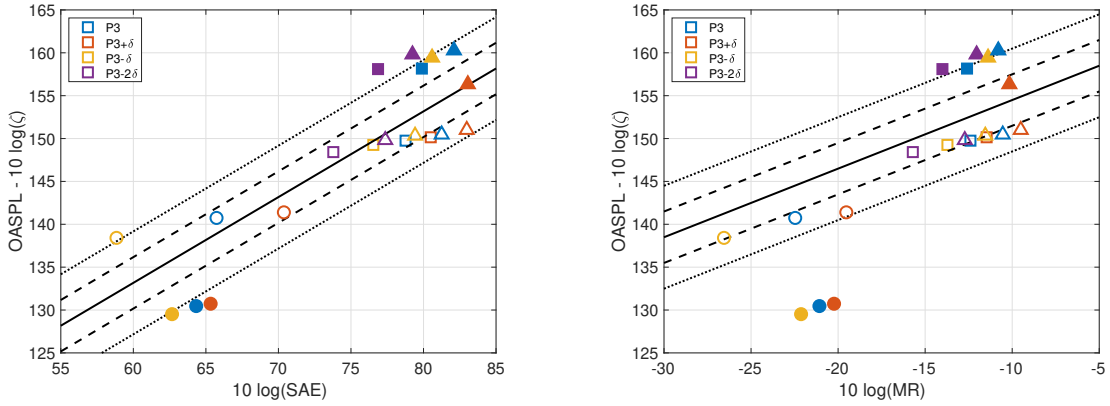

(a) (b)

Fig. 18 Comparison of measurements with legacy scaling laws for both N and N+3 cycle points, P_3 sweeps: (a) ANOPP/SAE model and (b) Mathew-Rekos model

same as in Fig. 16. The value of δ is 20 psi (137.9 kPa) for the N+3 approach case and in all other cases it is 50 psi (344.7 kPa). Again, the N-configuration data appear to cluster better around a straight line in the Mathews-Rekos plot than in the corresponding SAE/ANOPP plot. For the N+3 takeoff case, the increase in inlet total pressure, contrary to expectation, reduces the acoustic power. This is related to a reduction of the contributions from the 200 Hz and 250 Hz bands. These bands can be affected by the first two harmonics of the plunger-leakage mode. It is suggested here that the pressure increase stabilizes the flame and thereby reduces the influence of these harmonics.

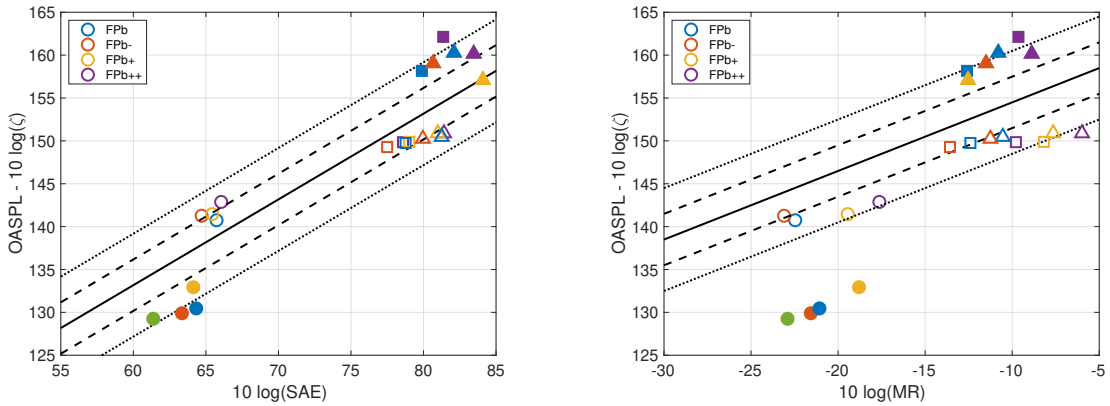

(a) (b)

Fig. 19 Comparison of measurements with legacy scaling laws for both N and N+3 cycle points, FP_b sweeps: (a) ANOPP/SAE model and (b) Mathew-Rekos model

Figure 19 shows the results for the combustor flow parameter (FP_b) sweeps. The blue, red, and gold colors indicate the nominal value at each operating point, a 10 % decrease, a 12.5 % increase, and a 25 % increase. The green color (only for the the N+3 approach case) indicates a 20 % decrease from the FP_b cycle value. The other keys are the same as in Fig. 16. Again, both legacy scaling laws tend to give reasonable predictions for the N configuration. It is interesting to note that if the systematic over prediction of about 4.5 dB is ignored, the Mathews-Rekos formula gives the smallest scatter around a straight line. However, the goodness should not be judged solely on the results from one particular parameter sweep. Apart from the gold triangle (takeoff), the trends for the N+3 configuration are correctly predicted.

V. Summary

A first-of-its-kind database [5] of detailed unsteady measurements characterizing noise sources of an advanced (N+3) low-emissions aero-combustor design has been further analyzed. The over all program [5] addressed the need for fundamental combustion noise experiments through testing in a combustor rig at relevant pressures and temperatures. In addition to the advanced N+3 layout, a reference configuration with the test section arranged to model an N (RQL-type) combustor sector was also studied. The present paper assesses the impact on legacy semi-empirical noise-prediction methods resulting from the N+3 radical departure from N combustor operating conditions and designs, such as fuel-air distribution and flame anchoring techniques. In the near term, the generated data and physical understanding will enable improvements to reduced-order models for use in system level noise assessments at the preliminary design stage for advanced air transport vehicles. In the long term, the database [5] can provide validation of high-fidelity prediction methods suited for detailed multidisciplinary acoustics/emissions combustor design.

For the test rig in the N-generation configuration, it was found that the measured broadband acoustic data were reasonably well described by acoustic-power scaling laws used in legacy semi-empirical noise-prediction methods. For the N+3 configuration, the legacy scaling laws, with some notable exceptions, provided correct trends, but with much less accuracy compared to the N configuration. Contrary to expectations, positive fuel-to-air ratio excursions were found reduce the noise levels (apparently by improving the main flame stability) and actually brought acoustic power levels closer to legacy-scaling-law values. In fact, any parameter sweep (e.g. lowering the combustor inlet total temperature T_3) that lessened the main-flame stability tended to increase the noise level. Such insights may suggest broadband combustor noise reduction strategies for advanced aero-combustors.

It is important to point out that the design experience and rules for N-type combustors are relatively well established by now since their development begun in the mid to late 1990s. However, the corresponding statement cannot be made for the future advanced N+3 combustors still in their early stages of research and development. It is speculated here that, as the N+3 design experience grows (particularly in respect to main-flame stabilization), the legacy scaling laws for broadband acoustic power might also become adequeate for early system-based design studies for N+3-type combustors.

References

[1] Mongeau, L., Huff, D., and Tester, B. J., "Aircraft Noise Technology Review and Medium and Long Term Noise Reduction Goals," *ICA 2013 Montreal*, 2013. doi:10.1121/1.4800944.

[2] Berton, J. J., Envia, E., and Burley, C. L., "An Analytical Assessment of NASA's N+1 Subsonic Fixed Wing Project Noise Goal," AIAA Paper 2009-3144, 16th AIAA/CEAS Aerocoustics Conference, Miami, Florida, 2009. doi:10.2514/6.2009-3144.

[3] Smith, L. L., "Fuel Flexible Combustor for High-OPR Compact-Core N+3 Propulsion Engine," Contractor Report NASA/CR–2020-220498, NASA, 2020. URL https://ntrs.nasa.gov/citations/20200001621.

[4] He, Z. J., Capil, T. G., Chang, C. T., Podboy, D., and Smith, L. L., "Emission Characteristics of an Axially Staged Sector Combustor for a Small Core High OPR Subsonic Aircraft Engine," AIAA Paper 2020-0627, AIAA SciTech 2020 Forum, Orlando, Florida, 2020. doi:10.2514/6.2020-0627.

[5] McCormick, D., Snyder, J., Kim, W., and Mendoza, J. M., "Acoustics of Future Low-Emissions Combustor Technology, Volume 1: Final Report," Contractor Report NASA/CR-20205011099/VOL1, NASA, 2020. URL https://ntrs.nasa.gov/citations/20205011099.

[6] Hultgren, L. S., "Semi-Empirical Modeling and Prediction of Direct Combustor Noise," Tech. Rep. NASA/TM–2018-220041, NASA, 2018.

[7] McKinney, R. G., Sepulveda, D., Sowa, W., and Cheung, A. K., "The Pratt & Whitney TALON X Low Emissions Combustor: Revolutionary Results with Evolutionary Technology," AIAA Paper 2007-0386, 45th AIAA Aerospace Sciences Meeting and Exhibit, Reno, Nevada, 2007. doi:10.2514/6.2007-386.

[8] Kramer, S., "NASA N+2 Advanced Low NOx Combustor Technology," Contractor Report NASA/CR–2020-220488, NASA, 2020. URL https://ntrs.nasa.gov/citations/20200002034.

[9] He, Z. J., Wey, C., Chang, C. T., C.-M., L., Surgenor, A. D., Kopp-Vaugham, K., and Cheung, A., "Emission Characteristics of a P & W Axially Staged Sector Combustor," AIAA Paper 2016-2121, 54th AIAA Aerospace Sciences Meeting, San Diego, California, 2016. doi:10.2514/6.2016-2121.

[10] Lee, C.-M., Chang, C. T., Kramer, S., and Herbon, J. T., "NASA Project Develops Next Generation Low-Emissions Combustor Terchnologies," AIAA Paper 2013-0540, 51st AIAA Aerospace Meeting, Grapevine (Dallas/Ft. Worth Region), Texas, 2013. doi:10.2514/6.2013-540.

[11] Liu, Y., Sun, X., Sethi, V., Nalianda, D., Li, Y.-G., and Wang, L., "Review of Modern Low Emissions Combustion Technologies for Aero Gas Turbine Engines," *Prog. Aerosp. Sci.*, Vol. 94, 2017, pp. 12–45. doi:10.1016/j.paerosci.2017.08.001.

[12] Duran, I., Moreau, S., Nicoud, F., Livebardon, T., Bouty, E., and Poinsot, T., "Combustion Noise in Modern Aero-Engines," *Aerospace Lab Journal*, Vol. 7-05, 2014, pp. 1–11, (DOI: 10.12762/2014.AL07–05).

[13] Dowling, A. P., and Mahmoudi, Y., "Combustion Noise," *Proceedings of the Combustion Institute*, Vol. 35, 2015, pp. 65–100. doi:10.1016/j.proci.2014.08.016.

[14] Ihme, M., "Combustion and Engine-Core Noise," *Annual Review of Fluid Mechanics*, Vol. 49, 2017, pp. 277–310. doi: 10.1146/annurev-fluid-122414-034542.

[15] Tam, C. K. W., Bake, F., Hultgren, L. S., and Poinsot, T., "Combustion Noise: Modeling and Prediction," *CEAS Aeronautical J.*, Vol. 10, No. 1, 2019, pp. 101–122. doi:10.1007/s13272-019-00377-2.

[16] O'Brien, J., Kim, J., and Ihme, M., "Integrated Analysis of Jet-Engine Core Noise Using a Hybrid Modeling Approach," AIAA Paper 2015-2821, 21st AIAA/CEAS Aeroacoustic Conference, Dallas, Texas, 2015. doi:10.2514/6.2015-2821.

[17] O'Brien, J., Kim, J., and Ihme, M., "Investigation of the Mechanisms of Jet-Engine Core Noise Using Large-Eddy Simulation," AIAA Paper 2016-0761, 54th AIAA Aerospace Sciences Meeting, San Diego, California, 2016. doi:10.2514/6.2016-0761.

[18] Livebardon, T., Moreau, S., Gicquel, L., Poinsot, T., and Bouty, E., "Combining LES of Combustion Chamber and an Actuator Disk Theory to Predict Combustion Noise in a Helicopter Engine," *Combust. Flame*, Vol. 165, 2016, pp. 272–287. doi:10.1016/j.combustflame.2015.12.012.

[19] Mathews, D. C., and Rekos, Jr, N. F., "Prediction and Measurement of Direct Combustion Noise in Turbopropulsion Systems," *J. Aircraft*, Vol. 14, No. 9, 1977, pp. 850–859. doi:10.2514/3.58865.

[20] Ho, P. Y., and Doyle, V. L., "Combustion Noise Prediction Update," AIAA Paper 1979-0588, 5th AIAA Aerocoustics Conference, Seattle, Washington, 1979. doi:10.2514/6.1979-588.

[21] Society of Automotive Engineers International, "Gas Turbine Jet Exhaust Prediction," Technical Standard (Aerospace Recommended Practice) SAE ARP876 Rev. E, 2006 (Reaffirmed 2012). doi:10.4271/ARP876E.

[22] Zorumski, W. E., "Aircraft Noise Prediction Program Theoretical Manual, Part 1," Tech. Rep. NASA-TM-83199-PT-1, NASA, 1982.

[23] Zorumski, W. E., "Aircraft Noise Prediction Program Theoretical Manual, Part 2," Tech. Rep. NASA-TM-83199-PT-2, NASA, 1982.

[24] Lord, W. K., Suciu, G. L., Hasel, K. L., and Chandler, J. M., "Engine Architecture for High Efficiency at Small Core Size," AIAA Paper 2015-0071, 53rd AIAA Aerospace Sciences Meeting, Kissimmee, Florida, 2015. doi:10.2514/6.2015-0071.